Cellular/Molecular

Astrocytic Gq-GPCR-Linked IP_3R-Dependent Ca^{2+} Signaling Does Not Mediate Neurovascular Coupling in Mouse Visual Cortex *In Vivo*

Daniel E. Bonder[1] **and Ken D. McCarthy**[2]

[1]Neurobiology Curriculum and [2]Department of Pharmacology, University of North Carolina at Chapel Hill, Chapel Hill, North Carolina 27599

Local blood flow is modulated in response to changing patterns of neuronal activity (Roy and Sherrington, 1890), a process termed neurovascular coupling. It has been proposed that the central cellular pathway driving this process is astrocytic Gq-GPCR-linked IP_3R-dependent Ca^{2+} signaling, though *in vivo* tests of this hypothesis are largely lacking. We examined the impact of astrocytic Gq-GPCR and IP_3R-dependent Ca^{2+} signaling on cortical blood flow in awake, lightly sedated, responsive mice using multiphoton laser-scanning microscopy and novel genetic tools that enable the selective manipulation of astrocytic signaling pathways *in vivo*. Selective stimulation of astrocytic Gq-GPCR cascades and downstream Ca^{2+} signaling with the hM3Dq DREADD (designer receptors exclusively activated by designer drugs) designer receptor system was insufficient to modulate basal cortical blood flow. We found no evidence of observable astrocyte endfeet Ca^{2+} elevations following physiological visual stimulation despite robust dilations of adjacent arterioles using cyto-GCaMP3 and Lck-GCaMP6s, the most sensitive Ca^{2+} indicator available. Astrocytic Ca^{2+} elevations could be evoked when inducing the startle response with unexpected air puffs. However, startle-induced astrocytic Ca^{2+} signals did not precede corresponding startle-induced hemodynamic changes. Further, neurovascular coupling was intact in lightly sedated, responsive mice genetically lacking astrocytic IP_3R-dependent Ca^{2+} signaling (IP_3R2 KO). These data demonstrate that astrocytic Gq-GPCR-linked IP_3R-dependent Ca^{2+} signaling does not mediate neurovascular coupling in visual cortex of awake, lightly sedated, responsive mice.

Key words: **astrocyte; blood flow; calcium; DREADD; *in vivo*; IP3**

Introduction

Understanding how cerebral vascular dynamics are coupled to neuronal activity is of intense scientific and clinical interest. Blood flow changes serve as the basis for functional MRI (Kim and Ogawa, 2012), which is the best method for noninvasively imaging human brain activity in real time. The underlying cellular and molecular mechanisms driving neurovascular coupling have remained elusive and controversial (Mishra et al., 2011; Nizar et al., 2013; Takata et al., 2013).

Substantial evidence using pharmacological approaches to manipulate astrocytic signaling *in situ* supports the hypothesis that functional hemodynamics are mediated by Gq-GPCR-linked Ca^{2+}-dependent processes (Zonta et al., 2003; Mulligan and MacVicar, 2004; Metea and Newman, 2006; Straub et al., 2006; Gordon et al., 2008; Girouard et al., 2010; He et al., 2012; Stobart et al., 2013). It remains unknown to what degree functional hemodynamics in the acute slice mirror processes of neurovascular coupling *in vivo*. It was recently reported that cortical arteriole dilations in anesthetized mice occur in the absence of observable Ca^{2+} elevations in adjacent astrocyte compartments (Nizar et al., 2013).

It is also unclear whether traditional experimental tools reveal physiology or artifacts of nonphysiological manipulations (Fiacco et al., 2007; Agulhon et al., 2010; Wang et al., 2013). Whereas chelating astrocytic Ca^{2+} blocks neurovascular coupling *in situ* (Mulligan and MacVicar, 2004; Gordon et al., 2008), functional hyperemia is intact in anesthetized IP_3R2 KO mice (Nizar et al., 2013; Takata et al., 2013), in which astrocytic IP_3R-dependent Ca^{2+} signaling is eliminated (Petravicz et al., 2008). However, astrocytic behavior could be markedly altered by anesthetics (Thrane et al., 2012). Anesthesia is known to increase basal blood flow in brain and alter functional hyperemia (Masamoto et al., 2009). Consequently, accurate dissection of the pathways mediating neurovascular coupling requires the development and application of models that enable experimentation under near-physiological conditions.

In this study, we used cutting-edge genetic tools and physiological stimuli to test the hypothesis that astrocytic Gq-GPCR-linked IP_3R-dependent Ca^{2+} signaling mediates neurovascular coupling in awake, lightly sedated, responsive mice. We used the hM3Dq DREADD (designer receptors exclusively activated by

Received June 25, 2014; revised Aug. 8, 2014; accepted Aug. 12, 2014.

Author contributions: D.E.B. and K.D.M. designed research; D.E.B. performed research; D.E.B. analyzed data; D.E.B. wrote the paper.

This work was supported by the National Eye Institute (R01EY021190-01 to K.D.M.) and the National Institute of Neurological Disorders and Stroke (5F31NS083329-02 to D.E.B.). Additionally, we thank Kristi Boyt (University of North Carolina at Chapel Hill) for preparation of AAV constructs and Dr. Spencer Smith (University of North Carolina at Chapel Hill) for his guidance in designing Matlab routines for imaging analysis.

The authors declare no competing financial interests.

Correspondence should be addressed to Ken D. McCarthy, Department of Pharmacology, University of North Carolina at Chapel Hill, Chapel Hill, NC 27599. E-mail: Ken_McCarthy@med.unc.edu.

DOI:10.1523/JNEUROSCI.2591-14.2014

 0270-6474/14/3313139-12$15.00/0

designer drugs) designer receptor system (Armbruster et al., 2007; Agulhon et al., 2013) to selectively stimulate astrocytic Gq-GPCR signaling cascades *in vivo*. To selectively eliminate IP_3R-dependent Ca^{2+} release downstream of Gq-GPCR activity, we used the IP_3R2 KO mouse model (Petravicz et al., 2008). These genetic technologies overcome the major limitations of pharmacological tools, such as nonselective drugs, caged molecules, or chelators, and enable precise control over astrocytic Gq-GPCR-linked IP_3R-dependent Ca^{2+} signaling *in vivo*. In addition to cell-permeable Ca^{2+} dyes, we used genetically encoded Ca^{2+} sensors, cyto-GCaMP3, and Lck-GCaMP6s for enhanced detection of astrocytic Ca^{2+} dynamics (Chen et al., 2013; Shigetomi et al., 2013). Overall, our experimental approach represents a significant advance over previous methods.

Our results establish that astrocytic Gq-GPCR-linked IP_3R-dependent Ca^{2+} signaling is not a central mediator of neurovascular coupling in visual cortex of lightly sedated, responsive mice. Additionally, our study introduces an experimental approach and genetic tools that can facilitate *in vivo* investigation on the cellular mechanisms that underlie functional hyperemia under near-physiological conditions.

Materials and Methods

Mice. All mice were housed in the animal facilities at the University of North Carolina, Chapel Hill, in accordance with Institutional Animal Care and Use Committee guidelines. IP_3R2 KO mice were generated as described previously (Li et al., 2005). $IP_3R2^{+/-}$ mice were interbred to generate homozygous full-mutant mice ($IP_3R2^{-/-}$) and littermate controls ($IP_3R2^{+/+}$). GFAP-cre mice were provided by Dr. Michael Sofroniew of the University of California at Los Angeles. The Gfap-cre transgene was designed containing Cre recombinase and the entire mouse glial fibrillary acidic protein (*/Gfap/*) gene, driven by the Gfap promoter sequence, as described previously (Gregorian et al., 2009). All mice were maintained on a C57BL/6 background and C57BL/6 littermates were used as wild-type controls. Both males and females were used for all studies.

Adeno-associated viral injection for expression of GCaMP or hM3Dq. Postnatal day (P) 45 to P90 mice were anesthetized with isoflurane (3–4% for induction, 1–2% for surgery, 100% oxygen). A vertical incision was made slightly lateral to midline, exposing primary visual cortex. The skull directly above the injection site was thinned to allow penetration by a glass pipette containing adeno-associated virus (AAV) diluted in cortex buffer artificial CSF (Holtmaat et al., 2009). Using a Harvard Apparatus 11 Plus pump and a syringe-to-pipette coupling system (Hamilton #55751-01), 0.5–1 μl of AAV solution was injected at a rate of 0.05 μl/min. AAVs were injected at the following titers: AAV8-GFAP-GCaMP3 and AAV8-GFAP-Lck-GCaMP6s, $1–1.2 \times 10^{10}$ genome copies/μl; AAV8-GFAP-DIO-GqDREADD-mCherry, 1×10^9 genome copies/μl. AAV was generated by the University of North Carolina Vector Core Services. Following successful injection, the needle was left in the cortex for ≥5 min to allow for diffusion of the AAV away from the needle track. The incision was sealed with Vetbond and a surgical staple, covered with antibiotic ointment, and mice were given a single injection of antibiotic subcutaneously (ciprofloxacin, 5 mg/kg body weight dose). Four weeks were given to allow for full transduction of virally delivered genes and sufficient regrowth of thinned section of skull before installation of chronic optical windows.

Chronic optical imaging through polished, reinforced thinned-skull windows. Naive adult mice or mice injected with AAV ≥4 weeks previously were anesthetized with isoflurane (3–4% for induction, 1–2% for surgery, 100% oxygen). Body temperature was maintained at 37.4°C (Fine Science Tools TR-200). Polished, reinforced thinned-skull (PoRTS) optical windows were prepared as previously described (Drew et al., 2010), with a minor modification. Following skull thinning with a high-speed drill (Foredom), we polished using a silicone whip coated with grit powder. We found this technique more suitable than polishing by agitating grit slurry with a silicone whip, which tended to push grit powder through the weakened part of the bone where the glass pipette had previously punctured when delivering AAV. Coating the silicone whip with grit created a gentler sanding device that was less likely to puncture the skull. Five days were given for recovery from surgery, and cortical structures ≤200–250 μm deep could be imaged for up to several months. This technique avoids the inflammation associated with chronic craniotomies (Xu et al., 2007; Drew et al., 2010) and offers greater convenience compared with traditional thinned-skull preparations, which require skull rethinning and enable only a few imaging experiments (Yang et al., 2010).

Fluorescence immunochemistry. Mice were perfusion fixed with 4% paraformaldehyde (PFA) in PBS 3 months after AAV injection and 2 months after PoRTS installation. Brains were removed and fixed in PFA for an additional 24 h, rinsed in PBS, placed in 30% sucrose in PBS solution for 24 h, frozen in Optimal Cutting Temperature compound, and cut in 40 μm sections on a Reichert-Jung Cryo-cut 1800 cryostat. Block solution (20% normal goat serum, 0.1% Triton X-100) was placed on the slides for 2 h at room temperature before antibody treatments. For astrocytic GFAP staining, a Cy3-conjugated mouse anti-GFAP monoclonal antibody (Sigma-Aldrich) was used at a 1:500 dilution in PBS. For microglial staining, a rabbit anti-Iba1 monoclonal antibody (Wako) was used at a 1:500 dilution in PBS. For enhancement of GCaMP signal, mouse (Sigma-Aldrich) or rabbit (Invitrogen), anti-GFP antibodies were used at 1:500 dilution. Primary antibodies remained on the slides for 24 h at 4°C, followed by appropriate secondary antibodies (Alexa Fluor) for 2 h at room temperature at a 1:1000 dilution in PBS. Sections were rinsed in PBS and mounted with Vectashield fluorescence mounting medium with DAPI (Vector). Widefield images were acquired on a Zeiss Axioskop.

In vivo *loading of Oregon Green BAPTA-1 and sulforhodamine-101 dye.* Adult mice (P60 to 6 months) were anesthetized with isoflurane (3–4% for induction, 1–2% for surgery, 100% oxygen). A 2–3-mm-diameter craniotomy was opened over primary visual cortex. The dura mater was left intact. A 50 μg aliquot of Oregon Green–BAPTA [1,2-bis-(*o*-aminophenoxy)ethane-*N*,*N*,*N*′,*N*′-tetra-acetatic acid]-1 (Invitrogen) was dissolved in a 20% Pluronic-127 (Invitrogen) solution in DMSO. After vortexing, this was diluted to 0.8 mM in cortex buffer containing 30 μM sulforhodamine 101 to label astrocytes (Nimmerjahn et al., 2004). Using similar methods as for AAV injection (see above), 40 nl of dye solution was injected at a depth of 250 μm. Placed over the craniotomy were 1.2% agarose gel and a 3 mm coverslip. The craniotomy was then sealed with dental cement (Parkell). For hydration and energy substrate, a subcutaneous injection of lactated Ringer's solution containing 5% dextrose was administered following surgery and before imaging.

Multiphoton imaging in lightly sedated, responsive mice. Initially, mice were anesthetized with isoflurane (3–4% for induction, 1–2% for maintenance, 100% oxygen). Chlorprothixene sedative was administered subcutaneously at doses between 0.4 and 3 mg/kg body weight. While anesthetized, mice were placed on a water-heated temperature-controlled pad (Adroit Medical, HTP-1500) and head-restrained underneath the microscope objective. In preparation for imaging, isoflurane was decreased and maintained well below anesthetizing levels (0–0.2%, 100% oxygen). The animal was allowed to stabilize under these conditions for ≥20 min before imaging. Under these conditions, mice are awake and responsive. They typically will not move during experiments, but if otherwise startled (by turning on the lights or touching the animal) they will struggle.

A custom two-photon microscope, converted from an Olympus Fluoview 300 system, with a 60×, 0.9 numerical aperture water-immersion objective and Hamamatsu photomultiplier tubes, was used for imaging. Images were acquired using Fluoview 300 software at 1–2 Hz. For OGB-1/SR-101 experiments, imaging was performed at an imaging resolution of 0.84 μm/pixel (240 × 180 pixels). For GCaMP experiments, resolution was 0.42 μm/pixel (480 × 420 pixels). High-speed line scanning (1.5 ms/line) was used to directly measure blood flow within individual cortical capillaries (see below). For experiments requiring clozapine-*N*-oxide (CNO) injection, a 30 gauge catheter was inserted intraperitoneally to permit injection of vehicle or CNO solution during imaging without touching or disturbing the animal.

Visual stimulation. VisionWorks software was used to generate drifting grating visual stimuli presented on a 7 inch VGA monitor (Lilliput

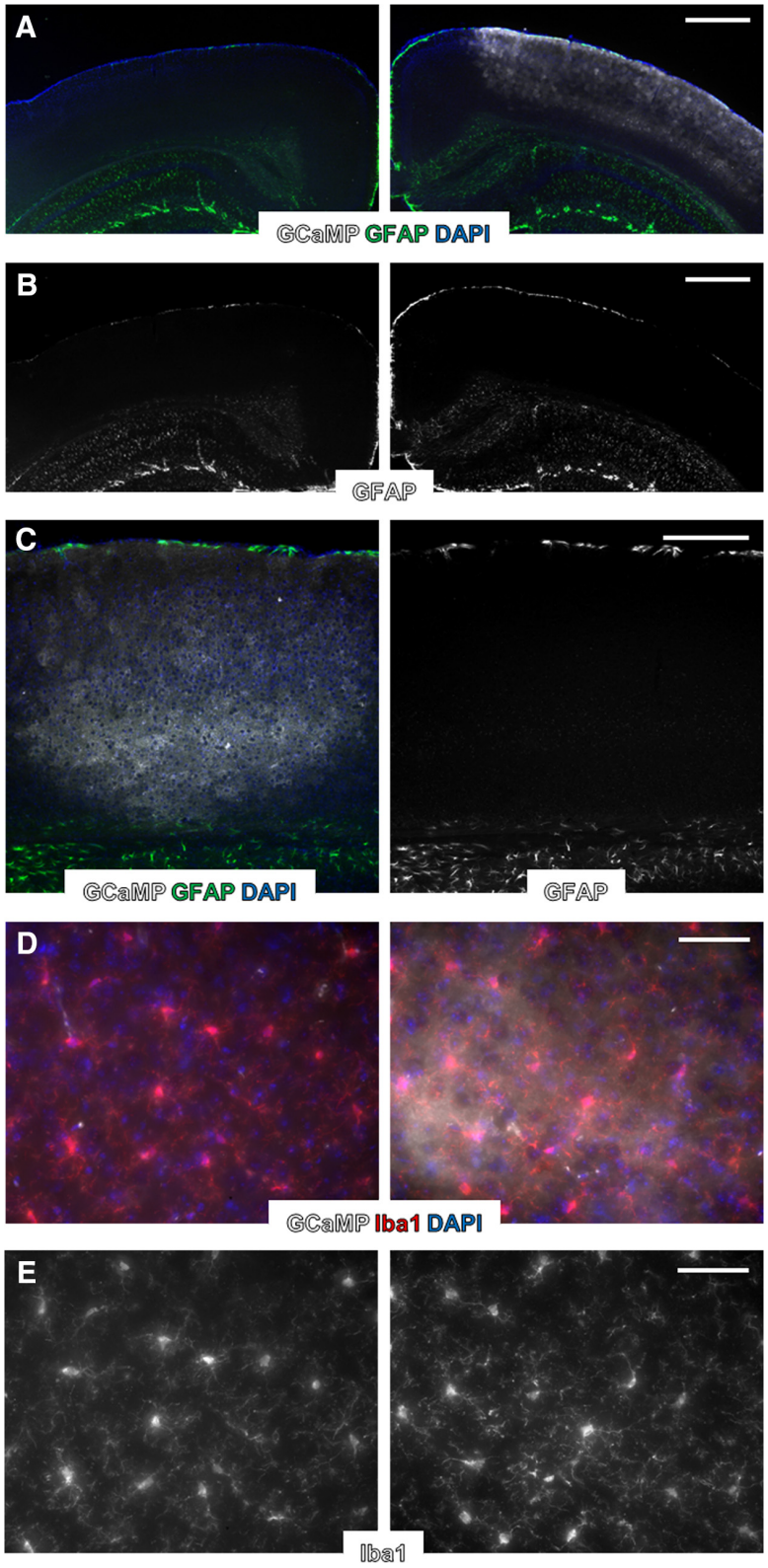

Figure 1. Expression of transgenes using AAV vectors does not lead to lasting astrocytic reactivity or microglial activation. ***A***, Fluorescence immunolabeling of nuclei (DAPI, blue), astrocytic GFAP (green), and Lck-GCaMP6s (gray) in visual cortex. Right, AAV-injected cortex. Left, Noninjected cortex from same animal. ***B***, Same images as in ***A*** but with GFAP only, more clearly displaying similarly sparse labeling in AAV-injected and noninjected cortices. ***C***, Fluorescence immunolabeling of nuclei (DAPI, blue), astrocytic GFAP (green), and Lck-GCaMP6s (gray) in visual cortex near the center of AAV injection and needle penetration. Right, GFAP only. ***D***, Fluorescence immunolabeling of nuclei (DAPI, blue), microglia (Iba1, red), and Lck-GCaMP6s (gray) in visual cortex. Right, AAV-injected cortex. Left, Noninjected cortex from same animal. ***E***, Same images as in ***D*** but with Iba1 only, more clearly displaying similar gross microglial morphology in AAV-injected and noninjected cortices. Scale bars: ***A***, ***B***, 500 μm; ***C***, 250 μm; ***D***, ***E***, 50 μm.

669GL) placed 10 cm from the mouse's eye at a 45° angle from normal. Stimuli consisted of 100% black/white contrast drifting square-wave gratings (spatial frequency, 0.05 cycles/°; drift speed, 2 cycles/s) presented at various angled orientations. A black, cardboard shroud was constructed and attached to the visual stimulus screen. This shroud fit just around the eye contralateral to optical window and prevented light from the stimulus screen from contaminating the imaging. Stimulus routines were designed such that orientations were presented in a unique, random order for each experimental set. Either short 5 s or longer 20 s stimuli were presented for all experiments. In the former case, orientations were 30° apart, for a total of 12 unique stimuli. In the latter case, orientations were 45° apart, for a total of 8 unique stimuli. Spike 2 software linked to a digitizer (Cambridge Electronic Design Micro 1401 DAQ) monitored outgoing triggers from the imaging acquisition system and the computer running VisionWorks.

Ca^{2+} imaging and analysis. ImageJ and Matlab software was used for image analysis. Image sequences were first motion-corrected using the Multistack Reg plugin for ImageJ. Ca^{2+} dynamics were obtained using custom Matlab scripts generously provided by Dr. Spencer Smith (University of North Carolina at Chapel Hill). These scripts allowed for semiautomated or freehand selection of regions of interest (ROIs). For OGB-1/SR-101 imaging data, ROIs were drawn around neuronal (OGB-1 positive, SR-101 negative) or astrocytic (OGB-1 positive, SR-101 positive) cell bodies. In the case of astrocytic ROIs, these were generated from the SR-101 channel to limit contamination from surrounding neuropil. The routine calculated the average pixel intensity $\Delta F/F_0$ with background noise subtracted for each ROI, and computed Ca^{2+} response averages based on precise trigger times tracked through Spike 2. Raw fluorescence data were mildly filtered using a five-point period exponential moving average function ($\alpha = ⅓$) before averaging multiple responses.

For GCaMP imaging data, ROIs were drawn around astrocyte endfeet adjacent to cortical arterioles. Arterioles could be identified based on two criteria: (1) arterioles display spontaneous vasomotion whereas venules do not, and (2) blood in postarteriole capillaries flows away from the vessel, whereas for venules blood flows toward the vessel. Arteriole dilations often caused endfeet to move in the *XY* plane, producing false fluorescence changes. This necessitated drawing enlarged ROIs to ensure that the entire endfoot remained within the ROI during arteriole dilations. Contamination from surrounding neuropil regions was not a concern as GCaMP was selectively expressed in astrocytes.

For sampling spontaneous astrocytic Ca^{2+} dynamics in a nonbiased manner (Fig. 1*B*; see Fig. 3*C*), we devised a grid analysis Matlab script. A grid of 20 × 20 pixel (~8.35 × 8.35 μm) box ROIs was tiled across the imaging field, with fluorescence changes extracted as described above.

Blood flow imaging and analysis. For imaging blood flow, a high molecular weight dextran-conjugated rhodamine dye (Sigma-Aldrich #R9379) was dissolved into a 5% solution with saline and injected into the tail vein. Blood flow was measured in two ways. First, as in Figures 1*C–E* and 3*E*,*F*, relative volumetric blood flow changes can be estimated based on the degree of arteriole diameter change in response to stimuli. The estimation involves use of the Hagen-Poiseuille equation of fluid dynamics, which states that volumetric flux varies as a function of the fourth power of the vessel radius. To ascertain estimates of changes in vessel radius, images of vascular rhodamine were filtered, using a two-pixel median filter, and binarized. Large ROIs were drawn around the vessel cross section. By tracking fluorescence changes of the binarized images, an area measurement in pixels was obtained. From this we derived changes in radius. Our estimated volumetric blood flow increases of 40 (see Figs. 3*D*,*E*, 4*B*) to 50% (see Fig. 3*F*) correspond to arteriole dilations of ~8–12% in diameter, similar to what has been described in other studies (Takano et al., 2006). Tracking arteriole dilations permits simultaneous monitoring of cellular Ca^{2+} dynamics and blood flow changes in response to stimuli *in vivo*.

Volumetric blood flow changes were also directly measured by tracking erythrocyte velocities within cortical capillaries (Schaffer et al., 2006), as in Figures 3*A* and 4*D*,*E*. Capillary diameters generally remain constant. Consequently, changes in blood velocity are directly proportional to changes in volumetric flux through the capillary. Erythrocyte velocities were determined by line scanning longitudinally through a length of capillary at high speed (1.5 ms/line). Matlab scripts, generously provided by Dr. Chris Schaffer (Cornell University), were used to calculate erythrocyte velocities from the resulting XT images. Compared with estimating changes in arteriole radius, this method of measuring blood flow is direct and has much greater temporal resolution.

Blood flow response onset was estimated by determining the X-intercept of a line drawn through two points along the rising phase of the response, at 20 and 80% of maximum. Unfiltered capillary line-scanning blood flow data were used for this analysis to obtain high temporal resolution.

Results

Selective stimulation of astrocytic hM3Dq does not alter basal visual cortical blood flow

Firmly elucidating the physiological role of astrocytic Gq-GPCR and Ca^{2+} signaling in neurovascular coupling has proven a difficult task due to reliance on pharmacological tools and acute slice preparations. To begin clarifying the role of astrocytic Gq-GPCR cascades and Ca^{2+} signaling in modulating cortical blood flow *in vivo*, we expressed the hM3Dq designer receptor and Lck-GCaMP6s in astrocytes using an AAV delivery system (see Materials and Methods). The hM3Dq viral construct included a double-inverted open reading frame element, which prohibits expression of hM3Dq in the absence of Cre-dependent recombination (Cardin et al., 2010). Astrocyte-selective expression of hM3Dq was therefore achieved by injecting the AAV into GFAP-Cre mice. Four weeks following AAV injection, mice were outfitted with a PoRTS cranial window (Drew et al., 2010), permitting chronic optical access to the visual cortex. Rhodamine dye was injected into the tail vein for monitoring changes in blood flow to stimuli based on direct measures within capillaries or arteriole diameter fluctuations (see Materials and Methods).

Expression of transgenes, such as GCaMP, using AAV vectors does not appear to alter astrocytic electrical properties or induce reactivity as assessed by GFAP immunolabeling (Haustein et al., 2014). We tested for clear signs of astrocytic or microglial reactivity under our experimental conditions with fluorescence immunostaining of astrocytic GFAP and microglia following AAV injection and installation of PoRTS optical windows. GFAP immunolabeling is typically sparse in adult mouse cortex (Nolte et al., 2001), but can be induced by trauma to the brain, such as a craniotomy procedure (Xu et al., 2007; Holtmaat et al., 2009). Under our experimental conditions, GFAP immunolabeling in the cortex ipsilateral to the AAV injection and PoRTS window were not detectably altered compared with the contralateral cortex (Fig. 1*A–C*; $n = 3$ mice). GFAP labeling remained sparse in AAV-injected cortex (Fig. 1*A*,*B*, right), similar to the noninjected contralateral cortex (Fig. 1*A*,*B*, left). This was true even near the center of AAV injection close to where the injection needle penetrated (Fig. 1*C*).

Altered microglial morphology is also indicative of cortical trauma (Xu et al., 2007). Iba1+ microglia from AAV-injected cortex (Fig. 1*D*,*E*, right) were indistinguishable from microglia in noninjected contralateral cortex (Fig. 1*D*,*E*, left) on the basis of gross morphology, indicating an absence of microglial reactivity near the injection and window site. These data suggest that expression of transgenes, such as Lck-GCaMP6s, in cortical astrocytes does not result in lasting glial reactivity.

Basal astrocytic Ca^{2+} activity in lightly sedated, responsive mice was readily detected by Lck-GCaMP6s (Fig. 2*A–C*; see Materials and Methods). Diverse types of astrocytic Ca^{2+} elevations, such as "single peaks," "multipeaks," or "plateaus," were detected throughout the imaging field (Fig. 2*C*). These signals arose with an average frequency of 0.182 ± 0.012 SEM events/min ($n = 3$ mice, 132 ROIs). Multipeak or plateau signals varied greatly in duration and so we focused further quantification on basal single-peak signals. The average basal single-peak signal and distribution of single-peak amplitudes are presented in Figure 2*D*,*E* ($n = 3$ mice, 92 Ca^{2+} signals).

In the following experiments, we focused on astrocyte endfeet (Fig. 2*A*, black arrow) adjacent to penetrating cortical arterioles (Fig. 2*A*, blue arrow). Intraperitoneal injection of CNO markedly increased astrocytic Ca^{2+} activity in mice expressing astrocytic hM3Dq (Fig. 2*F*), but not in wild-type mice (data not shown). The pattern of evoked Ca^{2+} elevation was dependent on CNO dose. Lower doses (typically 0.2 mg/kg) elicited "oscillatory-like" Ca^{2+} signals (Fig. 2*F*, top; $n = 6$ mice), whereas higher doses (typically 1 mg/kg) resulted in continuous "plateau-like" signals lasting several minutes (Fig. 2*F*, bottom; $n = 7$ mice). The latter of these signals has not been reported *in vivo* in response to physiological stimuli and likely reflects a supraphysiological stimulation of Gq-GPCR cascades. However, the kinetics of oscillatory-like CNO-evoked Ca^{2+} elevations closely mirrored those of basal single-peak elevations (Fig. 2, compare *D*, *G*, black trace). In addition, the average amplitude of CNO-evoked oscillatory-like Ca^{2+} elevations was within the range of amplitudes of basal single-peak signals (Fig. 2, compare *E*, *G*, black trace). These data suggest that the hM3Dq system is capable of evoking astrocytic Ca^{2+} elevations that fall within the physiological range of basal astrocytic Ca^{2+} dynamics in terms of kinetics and amplitude.

Despite the robust increase in astrocytic Ca^{2+} activity, basal blood flow remained unchanged following CNO injection (Fig. 2*F*). This was the case regardless of oscillatory-like (Fig. 2*F*, upper traces; $n = 6$ mice) or plateau-like (Fig. 2*F*, lower traces; $n = 7$ mice) responses. It was possible that blood flow was transiently modulated during individual endfoot Ca^{2+} elevations. To investigate this possibility, we determined blood flow changes during periods of elevated astrocytic Ca^{2+}. Cortical blood flow was unaffected by hM3Dq-induced Ca^{2+} increases in perivascular astrocyte endfeet, regardless of oscillatory-like (Fig. 2*G*; $n = 6$ mice, 37 Ca^{2+} elevations) or plateau-like responses (Fig. 2*H*; $n = 7$ mice, 7 Ca^{2+} elevations). Importantly, spontaneous arteriole vasomotion (fluctuation in arteriole diameter) was observed and functional hyperemia was readily evoked by physiological visual

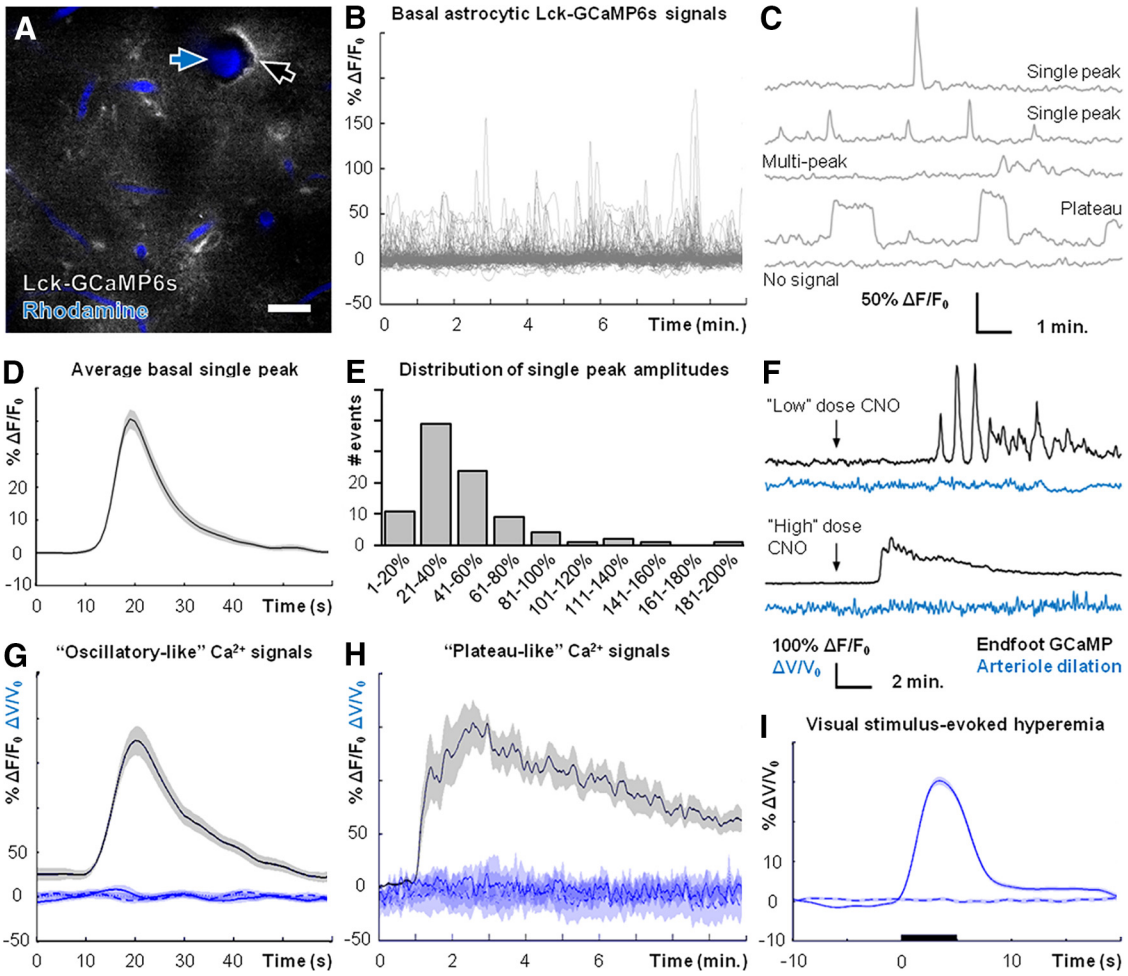

Figure 2. Basal cortical blood flow is unaffected by stimulation of astrocytic hM3Dq. ***A***, Field image of astrocytic Lck-GCaMP6s (gray) and intravascular rhodamine (blue), showing astrocyte endfeet (black arrow) and a cortical arteriole (blue arrow). ***B***, Nonbiased sampling of Lck-GCaMP6s using a grid analysis (see Materials and Methods) reveals robust basal astrocytic Ca^{2+} dynamics. ***C***, Representative examples of diverse basal astrocytic Ca^{2+} signals detected by Lck-GCaMP6s ($n = 3$ mice, 132 ROIs). ***D***, Average basal astrocytic single-peak Ca^{2+} elevation detected by Lck-GCaMP6s ($n = 3$ mice, 92 Ca^{2+} signals). ***E***, Histogram of basal astrocytic single-peak Ca^{2+} elevations detected by Lck-GCaMP6s ($n = 3$ mice, 92 Ca^{2+} signals). ***F***, Representative traces of different types of astrocytic Ca^{2+} responses (black traces) that can be evoked by adjusting CNO dose, and basal blood flow during same CNO trials (blue traces). ***G***, Average blood flow (solid blue line; $n = 6$ mice, 37 trials) during CNO-induced astrocytic oscillatory-like Ca^{2+} signals (black line; $n = 6$ mice, 37 Ca^{2+} elevations). Dashed and dotted blue lines are averages from vehicle-injection and baseline (no injection) trials respectively. ***H***, Same information as ***D*** but during CNO-induced astrocytic plateau-like Ca^{2+} signals ($n = 7$ mice, 7 trials). Dashed and dotted blue lines are averages from vehicle-injection and baseline (no injection) trials respectively. ***I***, Average cortical blood flow increase ($n = 7$ mice, 379 stimulus trials) following visual stimulation (black bar). Dashed trace is during no-stimulus trials ($n = 7$ mice, 384 trials). Scale bar: ***A***, 20 μm. Shaded regions in ***D***, ***G–I*** represent SEM.

stimuli (Fig. 2*I*; $n = 7$ mice, 379 stimulus trials). Therefore, the lack of blood flow modulation by CNO is not due to an inability to evoke blood flow changes in our recording conditions. These data suggest that selective stimulation of astrocytic Gq-GPCR cascades that evoke downstream Ca^{2+} signaling is not sufficient to modulate basal cortical blood flow in lightly sedated, responsive mice.

Visual cortical astrocytes do not display observable somatic Ca^{2+} elevations following visual stimulation

In the prior section, we provided a detailed analysis on the correlation between basal cortical blood flow *in vivo* during experimental elevations of astrocytic Gq-GPCR-linked Ca^{2+} signaling. Next, we characterized astrocytic Ca^{2+} dynamics following the presentation of physiological drifting grating visual stimuli to lightly sedated, responsive mice (Fig. 3*A*). Following an acute craniotomy surgical procedure, we loaded Layer II/III of the visual cortex with Oregon Green BAPTA-1 AM (OGB-1) and sulforhodamine-101 (SR-101) dye to monitor somatic neuronal and astrocytic Ca^{2+} dynamics during stimulus presentations (Fig. 3*A*).

Neuronal cell bodies exhibited elevations in intracellular Ca^{2+} that correlated with visual stimulus presentation (Fig. 3*B*, top, black traces, *C*; $n = 4$ mice, 87 cells, 3132 stimulus trials). A population of Layer II/III cortical neurons did not respond during visual stimuli but exhibited spontaneous Ca^{2+} spiking activity (Fig. 3*B*, bottom, gray traces; $n = 4$ mice, 82 cells). We termed this population "nonresponsive neurons." In a separate set of experiments, visual stimuli evoked robust increases in cortical blood flow within capillaries (Fig. 2*I*; $n = 7$ mice, 379 stimulus trials). These results serve as strong positive controls both for visual system responsiveness to the stimuli and the ability to evoke robust blood flow changes in lightly sedated, responsive mice.

Despite strong neuronal and blood flow responses to visual stimuli, a similar analysis did not reveal observable stimulus-correlated Ca^{2+} activity within astrocyte cell bodies (Fig. 3*B*, middle, blue traces; $n = 4$ mice, 35 cells). However, averaging

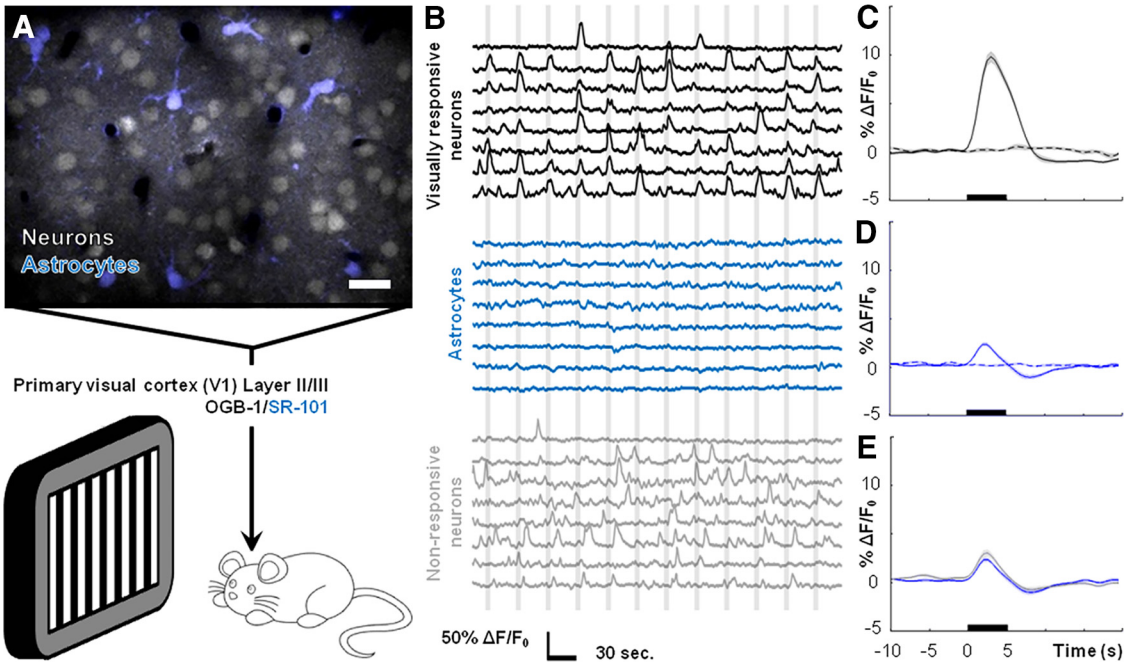

Figure 3. Mouse visual cortical astrocytes do not display observable somatic Ca^{2+} elevations following visual stimulation. ***A***, Field image showing Layer II/III neurons and astrocytes loaded with OGB-1 (gray)/SR-101 (blue) dye. Drifting grating visual stimuli were presented to lightly sedated, responsive mice. ***B***, Representative traces of fluorescence signals from ROIs drawn around the cell bodies of visually responsive neurons (black traces), astrocytes (blue traces), and visually nonresponsive neurons (gray traces) during stimulus presentations (vertical gray bars). ***C***, Average neuronal Ca^{2+} increase to visual stimuli ($n = 4$ mice, 87 cells, 3132 stimulus trials). ***D***, Average astrocytic Ca^{2+} dynamics during visual stimuli ($n = 4$ mice, 35 cells, 1152 stimulus trials). ***E***, Average astrocytic (blue) and nonresponsive neuronal (gray, $n = 4$ mice, 82 cells, 3132 stimulus trials) Ca^{2+} dynamics during visual stimuli, indicating contamination from neuropil signal. Scale bar: ***A***, 20 μm. For ***C–E***, stimuli were presented during time frame indicated by black bars, dashed lines indicate no-stimulus trials, and shaded regions represent SEM.

across all datasets identified a small, relatively rapid astrocytic Ca^{2+} response temporally correlated to the stimulus (Fig. 3*D*; $n = 4$ mice, 35 cells). Several points suggest that this response is contamination from neuropil signal in the Z-plane. First, averaging across datasets for the nonresponsive neuronal population reveals the same small, rapid Ca^{2+} elevation (Fig. 3*E*, gray trace; $n = 4$ mice, 82 cells, 3132 stimulus trials), suggesting a shared source of contamination. Second, the astrocytic signal was not observed when imaging GCaMP with expression restricted to astrocytes (Fig. 4*F–I*). In the absence of neuronal and neuropil indicator signal, no contamination effect was observed. Recent studies describe a similar contamination in their analyses of astrocytic Ca^{2+} dynamics *in vivo* (Lind et al., 2013; Nizar et al., 2013). These data demonstrate that astrocytes in lightly sedated, responsive mice do not display somatic Ca^{2+} elevations following visual stimulation.

Perivascular astrocyte endfeet do not display observable Ca^{2+} elevations following visual stimuli

It is increasingly appreciated that the larger share of astrocytic Ca^{2+} activity occurs in finer cellular processes ("microdomains") and not the soma (Di Castro et al., 2011; Panatier et al., 2011; Shigetomi et al., 2013; Sun et al., 2014; Volterra et al., 2014). It is believed that Ca^{2+} elevation within astrocyte endfeet is likely more crucial for mediating neurovascular coupling than Ca^{2+} signaling elsewhere in the cell (Attwell et al., 2010; Petzold and Murthy, 2011; Newman, 2013; Howarth, 2014). To monitor Ca^{2+} dynamics in astrocyte endfeet with enhanced sensitivity, we expressed cyto-GCaMP3 (Fig. 4*A*) or Lck-GCaMP6s (Fig. 2*A*) in astrocytes and simultaneously measured cellular Ca^{2+} signaling and blood flow changes following presentation of visual stimuli to lightly sedated, responsive mice.

Similar to Lck-GCaMP6s (Fig. 2*B*), cyto-GCaMP3 readily detected basal astrocytic Ca^{2+} dynamics (Fig. 4*B*) including single peaks, multipeaks, and plateaus (data not shown). These signals arose with an average frequency of 0.111 ± 0.01 SEM events/min ($n = 3$ mice, 181 ROIs). The decreased frequency of events revealed by cyto-GCaMP3 compared with Lck-GCaMP6s can most likely be attributed to the increased sensitivity of GCaMP6s (Chen et al., 2013), with additional sensitivity conferred by the membrane tethering of Lck-GCaMP6s (Shigetomi et al., 2013). The average basal single-peak Ca^{2+} signal detected using cyto-GCaMP3 (Fig. 4*C*; $n = 3$ mice, 94 Ca^{2+} signals) was similar kinetically to the average single peak detected using Lck-GCaMP6s (Figs. 2*D*, 4*D*). The slightly faster decay of the average single peak detected by cyto-GCaMP3 can most likely be attributed to the faster kinetic profile of GCaMP3 compared with GCaMP6s (Chen et al., 2013). The distribution of basal single-peak Ca^{2+} elevations detected by cyto-GCaMP3 is displayed in Figure 4*E* ($n = 3$ mice, 94 Ca^{2+} signals).

Surprisingly, astrocyte endfoot Ca^{2+} signals did not deviate from baseline values during visual stimuli even though cortical arterioles exhibited robust and reliable dilations (Fig. 4*F*; $n = 9$ mice). Ca^{2+} signals measured using cyto-GCaMP3 (Fig. 4*F*, top three black traces) were similar to those measured using Lck-GCaMP6s (Fig. 4*F*, bottom black trace). Clear arteriole dilations were observed regardless of GCaMP variant expressed (Fig. 4*F*, top, blue traces). Averaging across datasets confirmed that robust and reliable arteriole dilations occur in the absence of observable astrocyte endfoot Ca^{2+} elevations (Fig. 4*G*; $n = 9$ mice, 464 stimulus trials).

Recognizing that astrocytic Ca^{2+} elevations, when they do take place, are delayed relative to the onset of blood flow responses (Wang et al., 2006; Schummers et al., 2008; Tian et al., 2010), it has been suggested that, rather than playing a role in

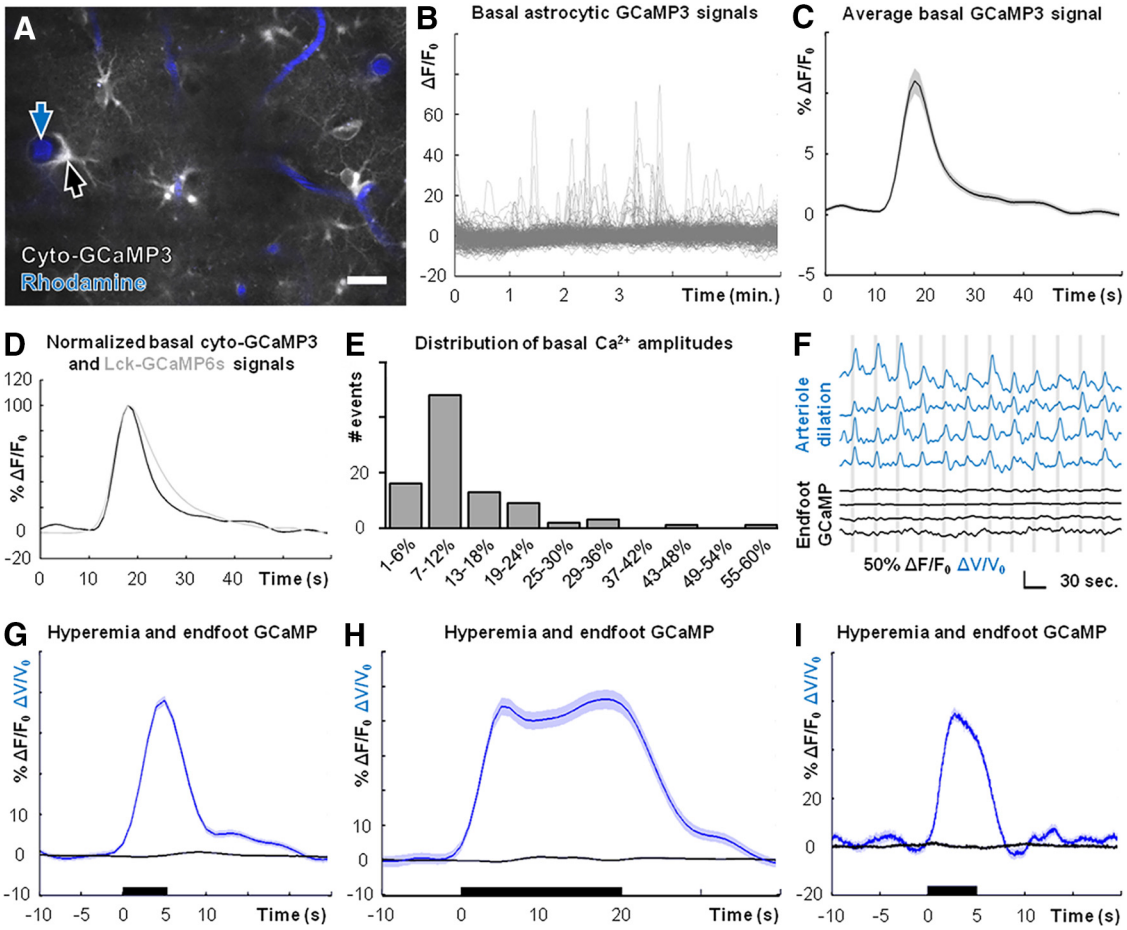

Figure 4. Cortical arterioles dilate in the absence of observable Ca^{2+} elevations in perivascular astrocyte endfeet. ***A***, Field image of cyto-GCaMP3 (gray) and intravascular rhodamine (blue), showing astrocyte endfeet (black arrow) and cortical arterioles (blue arrow). ***B***, Nonbiased sampling of cyto-GCaMP3 using a grid analysis (see Materials and Methods) reveals robust basal astrocytic Ca^{2+} dynamics. ***C***, Average basal astrocytic single-peak Ca^{2+} elevation detected by cyto-GCaMP3 ($n = 3$ mice, 94 Ca^{2+} signals). ***D***, Average basal astrocytic single-peak Ca^{2+} elevations detected by cyto-GCaMP3 (black trace) and Lck-GCaMP6s (gray trace; Fig. 2*D*), normalized to respective maxima. ***E***, Histogram of basal single-peak amplitudes detected by cyto-GCaMP3 ($n = 3$ mice, 94 Ca^{2+} signals). ***F***, Representative simultaneous measures of blood flow changes based on arteriole dilations (blue traces) and astrocyte endfoot Ca^{2+} dynamics (black traces) during visual stimulation (vertical gray bars). The top three traces for each are from experiments using cyto-GCaMP3. The bottom trace is from an experiment using Lck-GCaMP6s. ***G***, Average blood flow (blue trace, $n = 9$ mice, 464 stimulus trials) and astrocyte endfoot Ca^{2+} (black trace, $n = 9$ mice, 464 stimulus trials, pooled from cyto-GCaMP3 and Lck-GCaMP6s experiments) dynamics following 5-s-long visual stimuli (black bar). ***H***, Average blood flow (blue trace; $n = 5$ mice, 187 stimulus trials) and astrocyte endfoot Ca^{2+} (black trace; $n = 5$ mice, 187 stimulus trials, pooled from cyto-GCaMP3 and Lck-GCaMP6s experiments) dynamics following 20-s-long visual stimuli (black bar). ***I***, Average blood flow (blue trace) and astrocyte endfoot Ca^{2+} (black trace, Lck-GCaMP6s) dynamics assessed by high-speed multiphoton line scanning ($n = 3$ mice, 183 stimulus trials) following 5-s-long visual stimuli (black bar). Scale bar: ***A***, 20 μm. Shaded regions in ***C***, ***G–I*** represent SEM.

initiating functional hyperemia, astrocytic Ca^{2+} signaling might instead be important for maintaining or modulating blood flow during prolonged stimulus presentations (Schulz et al., 2012; Lind et al., 2013). However, we found no evidence of endfoot Ca^{2+} elevations when presenting 20-s-long stimuli (Fig. 4*H*; $n =$ 5 mice, 187 stimulus trials), compared with the earlier 5-s-long stimuli (Fig. 4*F*, *G*).

A recent study described a type of rapid, neuronal activity-dependent astrocytic Ca^{2+} signal (Lind et al., 2013). To test for the presence of this signal in visual cortical astrocytes following visual stimulation, we simultaneously imaged astrocyte endfoot Lck-GCaMP6s dynamics and arteriole dilations using high-speed line scanning (see Materials and Methods), achieving a temporal resolution of 3.5 ms per time point. We found no evidence of observable rapid Ca^{2+} elevations within astrocyte endfeet despite robust dilations of adjacent cortical arterioles (Fig. 4*I*; $n = 3$ mice, 183 stimulus trials). Together, these data suggest that arteriole diameter and cortical blood flow can be modulated in lightly sedated, responsive mice in the absence of observable Ca^{2+} elevations in astrocyte cell bodies or endfeet.

Startle-inducing air puff stimuli elicit astrocytic Ca^{2+} elevations and cortical blood flow changes

Despite both GCaMP variants readily detecting basal astrocytic Ca^{2+} signals (Figs. 2*B*, 4*B*), we were unable to observe positive Ca^{2+} elevations following visual stimulation (Figs. 3*D*, 4*F–I*). We next sought an alternative stimulation method that could reliably evoke astrocytic Ca^{2+} elevations under our experimental conditions and serve as a positive control. The cortex contains widespread noradrenergic projections from the locus ceruleus, and electrical stimulation of this nucleus readily elicits Ca^{2+} elevations in cortical astrocytes (Bekar et al., 2008). Noradrenergic projections to the cortex appear to play a prominent role in mediating concerted cortical astrocytic Ca^{2+} dynamics in fully awake mice, particularly when engaged through the startle response (Ding et al., 2013; Paukert et al., 2014). We therefore monitored visual cortical astrocytic Ca^{2+} dynamics with Lck-GCaMP6s while inducing the startle response with unexpected 3–4-s-long air puffs (Ding et al., 2013).

Startling lightly sedated, responsive mice with air puffs resulted in field-wide elevations of astrocytic Ca^{2+} (Fig. 5*A*; $n = 5$

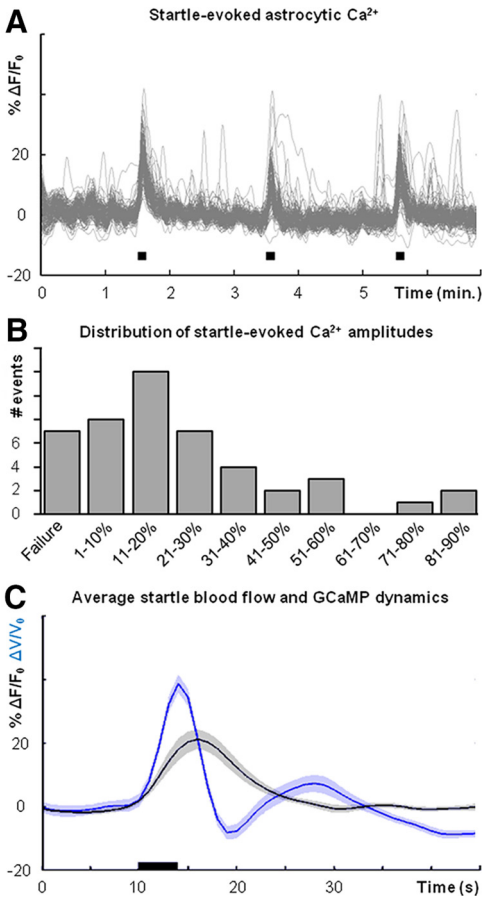

Figure 5. Air puff startle elicits widespread astrocytic Ca^{2+} elevation and cortical blood flow changes. ***A***, Nonbiased sampling of air puff (black boxes) startle-evoked astrocytic Ca^{2+} (Lck-GCaMP6s) signals using a field-wide grid analysis (see Materials and Methods). ***B***, Histogram of astrocytic Ca^{2+} elevation amplitudes following air puff startle ($n = 5$ mice, 46 stimulus trials). ***C***, Average blood flow changes (blue trace) and astrocyte endfoot Ca^{2+} signals (black trace, Lck-GCaMP6s) following air puff startle, indicated by black bar ($n = 5$ mice, 46 stimulus trials). Shaded regions in ***C*** represent SEM.

mice), thus demonstrating the ability of astrocytes to display Ca^{2+} elevations following a physiological stimulus under our experimental conditions. The distribution of response amplitudes is displayed in Figure 5*B*, with failures occurring in 7 of 46 total air puffs ($n = 5$ mice, 46 air puffs). Air puffs also elicited a distinct pattern of blood flow changes on average, with an initial increase followed by a dip below baseline, and a final recovery to baseline or slight overshoot (Fig. 5*C*, blue trace; $n = 5$ mice, 46 air puffs). Interestingly, on average the astrocytic Ca^{2+} elevations do not appear to precede the initial blood flow changes (Fig. 5*C*; $n = 5$ mice, 46 air puffs). These data indicate that startling lightly sedated, responsive mice with unexpected air puffs is sufficient to evoke widespread astrocytic Ca^{2+} elevations and alter cortical blood flow. However, astrocytic Ca^{2+} elevations do not precede the initial blood flow increase, suggesting that astrocytic Ca^{2+} signaling does not mediate the onset of vascular dynamics during the startle response.

Genetic deletion of astrocytic IP_3R-dependent Ca^{2+} signaling does not alter neurovascular coupling in lightly sedated, responsive mice

Two recent studies demonstrated that functional hyperemia is intact in anesthetized IP_3R2 KO mice *in vivo* (Nizar et al., 2013; Takata et al., 2013), in which astrocytic IP_3R-dependent Ca^{2+} activity is eliminated (Petravicz et al., 2008). Accurate interpretation of these results is difficult because of the confounding effects of anesthesia or anesthetized state on astrocytic signaling (Thrane et al., 2012) and blood flow dynamics (Masamoto et al., 2009). To determine whether functional hyperemia is altered in lightly sedated, responsive IP_3R2 KO mice, we loaded the visual cortex with OGB-1/SR-101 dye and monitored neuronal and astrocytic Ca^{2+} dynamics following visual stimulation in IP_3R2 KO mice and wild-type littermate controls.

Previous studies demonstrated that basal neuronal activity and plasticity are unaffected by the loss of astrocytic IP_3R-dependent Ca^{2+} signaling (Petravicz et al., 2008; Agulhon et al., 2010). Similarly, *in vivo* the percentage of total neurons sampled that were responsive to visual stimuli was not statistically different between IP_3R2 KO visual cortex and controls (Fig. 6*A*; $n = 4$ mice each genotype; wild type, $n = 169$ cells; KO, $n = 177$ cells; Student's t test, $p = 0.7328$). Average neuronal Ca^{2+} spiking response to visual stimulation did not differ between genotypes (Fig. 6*B*, $n = 4$ mice each genotype; wild type, $n = 87$ cells, 3132 stimulus trials; KO, $n = 88$ cells, 3168 stimulus trials). As anticipated, we did not observe Ca^{2+} elevations in astrocyte cell bodies from IP_3R2 KO mice (Fig. 6*C*, inset; $n = 4$ mice each genotype; wild type, $n = 35$ cells, 1152 stimulus trials; KO, $n = 30$ cells, 1080 stimulus trials). These data suggest that the visual cortical circuitry of IP_3R2 KO mice and wild-type littermate controls is similarly responsive to visual stimuli.

Functional hyperemia was completely intact in lightly sedated, responsive IP_3R2 KO mice following visual stimulus presentation (Fig. 6*D*; wild type, $n = 7$ mice, 379 stimulus trials; KO, $n = 8$ mice, 414 stimulus trials). Similar results were observed with 20-s-long visual stimulation (Fig. 6*E*; wild type, $n = 7$ mice, 189 stimulus trials; KO, $n = 6$ mice, 227 stimulus trials). Across a range of studies, observable astrocytic Ca^{2+} elevations in response to Gq-GPCR agonists (Petravicz et al., 2008; Chen et al., 2012; He et al., 2012; Navarrete et al., 2012; Nizar et al., 2013), electrical field stimulation (He et al., 2012; Wang et al., 2012; Haustein et al., 2014), or afferent stimulation (Takata et al., 2011; Navarrete et al., 2012; Nizar et al., 2013) are absent in IP_3R2 KO animals *in situ* and *in vivo*. Thus, these data suggest that astrocytic IP_3R-dependent Ca^{2+} signaling is not centrally involved in initiating functional hyperemia or modulating the sustained phase of neurovascular coupling in lightly sedated, responsive mice. Importantly, these data corroborate the critical results of recent *in vivo* studies (Nizar et al., 2013; Takata et al., 2013).

Discussion

Astrocytes are reported to alter vessel diameter by means of intracellular Ca^{2+} elevations (Attwell et al., 2010; Petzold and Murthy, 2011; Newman, 2013; Howarth, 2014). Astrocytes contact many synapses and astrocyte endfeet surround >99% of cerebral vascular surface (Mathiisen et al., 2010; McCaslin et al., 2011). It is hypothesized that neurotransmitter spillover from synapses stimulates astrocytic Gq-GPCRs, resulting in IP_3R-dependent Ca^{2+} release from endoplastic reticulum stores (Duffy and MacVicar, 1995; Porter and McCarthy, 1996; Araque et al., 2002; Newman, 2005) and Ca^{2+}-dependent release of vasoactive molecules onto arteriole smooth muscle (Zonta et al., 2003; Mulligan and MacVicar, 2004; Takano et al., 2006), thereby modulating blood flow. However, accurate dissection of the cellular pathways underlying neurovascular coupling has proven difficult. Mechanistic studies have relied on acute slice preparations and pharmacological tools with direct *in vivo* tests largely lacking.

A recent study questions our current mechanistic understanding of neurovascular coupling. Using dyes to monitor neuronal

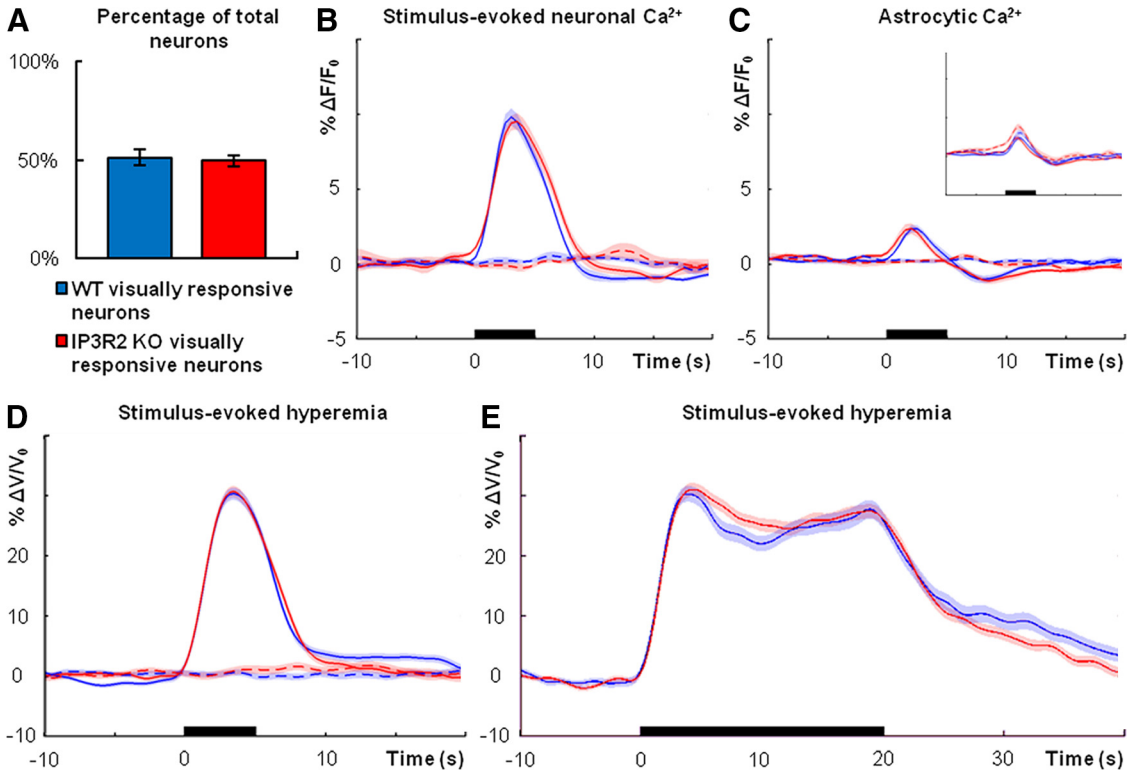

Figure 6. Neurovascular coupling is intact in visual cortex of lightly sedated, responsive IP_3R2 KO mice. ***A***, Percentage of neurons (OGB-1 positive/SR-101 negative) that are responsive to visual stimuli ($n = 4$ mice each genotype; wild type, $n = 169$ total cells; KO, $n = 177$ total cells; Student's t test, $p = 0.7328$). ***B***, Average neuronal Ca^{2+} increases in wild type (blue; $n = 4$ mice, 87 cells, 3132 stimulus trials) and IP_3R2 KO (red; $n = 4$ mice, 88 cells, 3168 stimulus trials) following 5-s-long visual stimulation (black bar). Dashed traces are averages from trials in which no stimuli were presented. ***C***, Average astrocytic Ca^{2+} dynamics following 5-s-long visual stimulation (black bar) in wild type (blue; $n = 4$ mice, 35 cells, 1152 stimulus trials) and IP_3R2 KO (red; $n = 4$ mice, 30 cells, 1080 stimulus trials). Dashed traces are averages from trials in which no stimuli were presented. Inset additionally displays wild-type (dashed blue trace) and IP_3R2 KO (dashed red trace) nonresponsive neuron Ca^{2+} signals during visual stimuli, indicating contamination from neuropil signal. ***D***, Average blood flow increase following 5-s-long visual stimulus (black bar) in wild type (blue; $n = 7$ mice, 379 stimulus trials) and IP_3R2 KO (red; $n = 8$ mice, 414 stimulus trials). Dashed traces are averages from trials in which no stimuli were presented. ***E***, Average blood flow increase to 20-s-long visual stimulus (black bar) in wild type (blue; $n = 7$ mice, 189 stimulus trials) and IP_3R2 KO (red; $n = 6$ mice, 227 stimulus trials). Dashed traces are averages from trials in which no stimuli were presented. Error bars in ***A*** and shaded regions in ***B–E*** represent SEM.

and astrocytic Ca^{2+} dynamics in anesthetized mice, Nizar et al. (2013) demonstrated that arteriole dilation could occur in the absence of observable endfoot Ca^{2+} elevation, that astrocytic Ca^{2+} elevations did not precede dilation of adjacent arterioles following footshock, and that arteriole dilations in IP_3R2 KO mice were intact. However, this study was limited by its reliance on computational processing to isolate astrocytic Ca^{2+} signal from contaminating neuropil signal and by the use of general anesthesia, which interferes with astrocytic signaling (Thrane et al., 2012) and alters brain blood flow (Masamoto et al., 2009).

Our study is the first using the DREADD designer receptor system, GCaMP, and chronic PoRTS optical windows for assessing the role of Gq-GPCR and Ca^{2+} signaling cascades in neurovascular coupling *in vivo* in the absence of general anesthesia, thereby representing a significant advance experimentally on numerous fronts. We analyzed the effects of selective manipulations of astrocytic Gq-GPCR and IP_3R-dependent signaling on neurovascular coupling in visual cortex of awake, lightly sedated, responsive mice, and simultaneously monitored vascular and astrocytic Ca^{2+} dynamics following visual stimulation. Our data strongly argue that astrocytic Gq-GPCR cascades and IP_3R-dependent Ca^{2+} signaling are neither sufficient nor necessary for functional hyperemia *in vivo*. These pathways do not play as central a role in neurovascular coupling as previously reported.

First, selective stimulation of astrocytic Gq-GPCR signaling cascades was not sufficient to modulate basal cortical blood flow *in vivo* (Fig. 2). Previous studies used bath application of Gq-GPCR agonists (Zonta et al., 2003; He et al., 2012), Ca^{2+} uncaging (Metea and Newman, 2006; Girouard et al., 2010; Stobart et al., 2013), or electrical afferent or field stimulation (Filosa et al., 2006; Girouard et al., 2010; He et al., 2012) to demonstrate that elevations in astrocytic Ca^{2+} are sufficient to alter vascular diameter *in situ*. Uncaging Ca^{2+} in endfeet is sufficient to modulate arteriole diameter *in vivo* (Takano et al., 2006). Whether pharmacological signaling manipulations *in situ* are representative of physiology is unclear. Receptor agonists are not cell-selective and could modulate vascular diameter through cell types other than astrocytes. Laser uncaging does not engage the full fabric of Gq-GPCR cascades. Acute slice preparations lack blood flow and intraluminal vascular pressure, and astrocytes might rapidly enter a state of reactive gliosis (Takano et al., 2014).

To overcome such concerns, we used the hM3Dq DREADD system (Armbruster et al., 2007). The hM3Dq enables stimulation of the entire Gq-GPCR cascade selectively in astrocytes *in vivo*, an advance over previous methods. The hM3Dq system has been successfully used by many investigators to dissect the contribution of cell-specific signaling cascades in physiological processes *in vivo* (Wess et al., 2013). We observed robust CNO-induced Ca^{2+} elevations within perivascular astrocyte endfeet in mice expressing hM3Dq in astrocytes, yet the diameters of adjacent arterioles remained at baseline values. Contrasting with previous studies, our observations indicate that stimulation of

astrocytic Gq-GPCR cascades is not sufficient to modulate basal cortical blood flow *in vivo*. It is possible that astrocytic Gq-GPCR signaling could modulate physiologically evoked hemodynamics, an interesting subject for future studies.

Second, arteriole dilations following visual stimulation occurred independently of observable Ca^{2+} elevations in astrocyte cell bodies (Fig. 3) and arteriole-adjacent endfeet (Fig. 4). We observed robust spontaneous Ca^{2+} dynamics when cyto-GCaMP3 or membrane-bound Lck-GCaMP6s was expressed in astrocytes. GCaMP3 allows for greater detection of microdomain Ca^{2+} events in astrocytes compared with bulk-loaded dyes (Shigetomi et al., 2013) and GCaMP6s is the most sensitive Ca^{2+} indicator currently available (Chen et al., 2013). In addition to Gq-GPCR-linked IP_3R-dependent events, basal Ca^{2+} currents through plasma membrane TRP (transient receptor potential)-family channels have been described (Shigetomi et al., 2012; Dunn et al., 2013). Endfoot TRPV4 channels might play a role in amplifying neurovascular responses by facilitating Ca^{2+}-induced Ca^{2+} release (Dunn et al., 2013). However, we found no evidence of observable Ca^{2+} elevations in astrocyte endfeet of lightly sedated, responsive mice following visual stimulation, indicating that observable arteriole-adjacent endfoot Ca^{2+} is not required for functional hyperemia *in vivo* regardless of the pathway engaged.

We detected positive astrocytic Ca^{2+} signals and blood flow changes when startling lightly sedated, responsive mice with unexpected air puffs (Fig. 5). Interestingly, the startle-evoked astrocytic Ca^{2+} signals did not precede the onset of the blood flow increases. However, it is possible that the blood flow decrease following the initial increase (Fig. 5*C*) could be mediated by astrocytic Ca^{2+}-dependent processes. It is known that norepinephrine levels in the cortex differentially regulate functional hemodynamics *in vivo* (Bekar et al., 2012). These effects could stem from direct action of astrocytes on blood vessels, or perhaps from astrocyte-driven modulation of local neuronal circuitry. It has been suggested that astrocytic Ca^{2+} signaling might play a more prominent role in mediating startle or stress networks, with less critical involvement in local sensory processing (Ding et al., 2013; Sun et al., 2013; Paukert et al., 2014), an idea consistent with our findings. It will be interesting to explore these possibilities in future studies.

Infusing BAPTA into perivascular astrocytes *in situ* blocks Ca^{2+} elevations to bath-applied Gq-GPCR agonists or laser uncaging and prevents arteriole dilation (Mulligan and MacVicar, 2004). Interfering with astrocytic Ca^{2+} dynamics with receptor antagonists reduces vascular response *in situ* (Filosa et al., 2006) and *in vivo* (Zonta et al., 2003; Takano et al., 2006). However, functional hyperemia in response to footshock (Nizar et al., 2013) or whisker stimulation (Takata et al., 2013) is intact in anesthetized IP_3R2 KO mice, in which astrocytic IP_3R-dependent Ca^{2+} signaling is eliminated (Petravicz et al., 2008). The IP_3R2 KO model has been used by numerous groups to study astrocytic IP_3R-dependent cellular processes *in situ* and *in vivo* (Petravicz et al., 2008; Di Castro et al., 2011; Takata et al., 2011; Chen et al., 2012; He et al., 2012; Navarrete et al., 2012; Wang et al., 2012; Nizar et al., 2013; Haustein et al., 2014).

We observed that neurovascular coupling was intact in lightly sedated, responsive IP_3R2 KO mice (Fig. 6), strongly indicating that astrocytic IP_3R-dependent Ca^{2+} signaling is not necessary for functional hyperemia *in vivo*. It is insightful that in IP_3R2 KO acute slices, vascular responses to agonists or electrical field stimulation are eliminated (He et al., 2012), a result opposite of our findings and those of two other *in vivo* studies (Nizar et al., 2013; Takata et al., 2013). It is plausible that mechanisms of neurovascular coupling or vascular responsiveness differ in acute brain slice compared with *in vivo*.

A recent study characterized rapid astrocytic Ca^{2+} signals following stimuli *in vivo*, the amplitude of which correlates with the amplitude of functional hyperemia (Lind et al., 2013). A previous study described rapid Ca^{2+} elevations (time to peak, ~0.5 s) in 5% of cortical astrocytes in anesthetized mice (Winship et al., 2007). Computational methods were used to isolate astrocytic Ca^{2+} signals from contaminating neuropil signals in both studies. In contrast, our use of GCaMP overcomes the problem of signal contamination by selectively labeling astrocytes. With Lck-GCaMP6s, we did not detect rapid Ca^{2+} signals in astrocytes following visual stimulation (Fig. 4). The presence or absence of rapid astrocytic Ca^{2+} signals may be a function of the strength of synaptic input to different cortical regions or of the nature and strength of stimulus used.

Our results strongly suggest that astrocytic Gq-GPCR-linked IP_3R-dependent Ca^{2+} signaling does not play a central role in mediating neurovascular coupling in the intact brain. Neuron-born mediators, perhaps involving the activity of specific interneuron subtypes (Cauli et al., 2004; Kocharyan et al., 2008; Cauli and Hamel, 2010), might be primary drivers of neurovascular coupling *in vivo*. It is also possible that astrocytes contribute to neurovascular coupling but through signaling processes other than Gq-GPCR-linked IP_3R-dependent Ca^{2+} elevation. Ionic processes have been proposed to mediate neurovascular coupling (Paulson and Newman, 1987; Witthoft et al., 2013). However, this possibility is relatively unexplored. Ion fluxes occur in concert with neurotransmitter uptake (Brew and Attwell, 1987; Langer and Rose, 2009) and ion buffering (Kofuji and Newman, 2004; Zhou et al., 2009) during local neuronal firing. In the future, it will be interesting to further elucidate these relatively underexamined cellular processes and assess potential roles they might have in mediating neurovascular coupling *in vivo*.

References

Agulhon C, Fiacco TA, McCarthy KD (2010) Hippocampal short- and long-term plasticity are not modulated by astrocyte Ca^{2+} signaling. Science 327:1250–1254. CrossRef Medline

Agulhon C, Boyt KM, Xie AX, Friocourt F, Roth BL, McCarthy KD (2013) Modulation of the autonomic nervous system and behaviour by acute glial cell Gq protein-coupled receptor activation in vivo. J Physiol 591:5599–5609. CrossRef Medline

Araque A, Martín ED, Perea G, Arellano JI, Buño W (2002) Synaptically released acetylcholine evokes Ca^{2+} elevations in astrocytes in hippocampal slices. J Neurosci 22:2443–2450. Medline

Armbruster BN, Li X, Pausch MH, Herlitze S, Roth BL (2007) Evolving the lock to fit the key to create a family of G protein-coupled receptors potently activated by an inert ligand. Proc Natl Acad Sci U S A 104:5163–5168. CrossRef Medline

Attwell D, Buchan AM, Charpak S, Lauritzen M, Macvicar BA, Newman EA (2010) Glial and neuronal control of brain blood flow. Nature 468:232–243. CrossRef Medline

Bekar LK, He W, Nedergaard M (2008) Locus coeruleus alpha-adrenergic-mediated activation of cortical astrocytes in vivo. Cereb Cortex 18:2789–2795. CrossRef Medline

Bekar LK, Wei HS, Nedergaard M (2012) The locus coeruleus-norepinephrine network optimizes coupling of cerebral blood volume with oxygen demand. J Cereb Blood Flow Metab 32:2135–2145. CrossRef Medline

Brew H, Attwell D (1987) Electrogenic glutamate uptake is a major current carrier in the membrane of axolotl retinal glial cells. Nature 327:707–709. CrossRef Medline

Cardin JA, Carlén M, Meletis K, Knoblich U, Zhang F, Deisseroth K, Tsai LH, Moore CI (2010) Targeted optogenetic stimulation and recording of neurons in vivo using cell-type-specific expression of Channelrhodopsin-2. Nat Protoc 5:247–254. CrossRef Medline

Cauli B, Hamel E (2010) Revisiting the role of neurons in neurovascular coupling. Front Neuroenergetics 2:9. CrossRef Medline

Cauli B, Tong XK, Rancillac A, Serluca N, Lambolez B, Rossier J, Hamel E (2004) Cortical GABA interneurons in neurovascular coupling: relays for subcortical vasoactive pathways. J Neurosci 24:8940–8949. CrossRef Medline

Chen N, Sugihara H, Sharma J, Perea G, Petravicz J, Le C, Sur M (2012) Nucleus basalis-enabled stimulus-specific plasticity in the visual cortex is mediated by astrocytes. Proc Natl Acad Sci U S A 109:E2832–E2841. CrossRef Medline

Chen TW, Wardill TJ, Sun Y, Pulver SR, Renninger SL, Baohan A, Schreiter ER, Kerr RA, Orger MB, Jayaraman V, Looger LL, Svoboda K, Kim DS (2013) Ultrasensitive fluorescent proteins for imaging neuronal activity. Nature 499:295–300. CrossRef Medline

Di Castro MA, Chuquet J, Liaudet N, Bhaukaurally K, Santello M, Bouvier D, Tiret P, Volterra A (2011) Local Ca2+ detection and modulation of synaptic release by astrocytes. Nat Neurosci 14:1276–1284. CrossRef Medline

Ding F, O'Donnell J, Thrane AS, Zeppenfeld D, Kang H, Xie L, Wang F, Nedergaard M (2013) α1-Adrenergic receptors mediate coordinated Ca2+ signaling of cortical astrocytes in awake, behaving mice. Cell Calcium 54:387–394. CrossRef Medline

Drew PJ, Shih AY, Driscoll JD, Knutsen PM, Blinder P, Davalos D, Akassoglou K, Tsai PS, Kleinfeld D (2010) Chronic optical access through a polished and reinforced thinned skull. Nat Methods 7:981–984. CrossRef Medline

Duffy S, MacVicar BA (1995) Adrenergic calcium signaling in astrocyte networks within the hippocampal slice. J Neurosci 15:5535–5550. Medline

Dunn KM, Hill-Eubanks DC, Liedtke WB, Nelson MT (2013) TRPV4 channels stimulate Ca2+-induced Ca2+ release in astrocytic endfeet and amplify neurovascular coupling responses. Proc Natl Acad Sci U S A 110:6157–6162. CrossRef Medline

Fiacco TA, Agulhon C, Taves SR, Petravicz J, Casper KB, Dong X, Chen J, McCarthy KD (2007) Selective stimulation of astrocyte calcium in situ does not affect neuronal excitatory synaptic activity. Neuron 54:611–626. CrossRef Medline

Filosa JA, Bonev AD, Straub SV, Meredith AL, Wilkerson MK, Aldrich RW, Nelson MT (2006) Local potassium signaling couples neuronal activity to vasodilation in the brain. Nat Neurosci 9:1397–1403. CrossRef Medline

Girouard H, Bonev AD, Hannah RM, Meredith A, Aldrich RW, Nelson MT (2010) Astrocytic endfoot Ca2+ and BK channels determine both arteriolar dilation and constriction. Proc Natl Acad Sci U S A 107:3811–3816. CrossRef Medline

Gordon GR, Choi HB, Rungta RL, Ellis-Davies GC, MacVicar BA (2008) Brain metabolism dictates the polarity of astrocyte control over arterioles. Nature 456:745–749. CrossRef Medline

Gregorian C, Nakashima J, Le Belle J, Ohab J, Kim R, Liu A, Smith KB, Groszer M, Garcia AD, Sofroniew MV, Carmichael ST, Kornblum HI, Liu X, Wu H (2009) *Pten* deletion in adult neural stem/progenitor cells enhances constitutive neurogenesis. J Neurosci 29:1874–1886. CrossRef Medline

Haustein MD, Kracun S, Lu XH, Shih T, Jackson-Weaver O, Tong X, Xu J, Yang XW, O'Dell TJ, Marvin JS, Ellisman MH, Bushong EA, Looger LL, Khakh BS (2014) Conditions and constraints for astrocyte calcium signaling in the hippocampal mossy fiber pathway. Neuron 82:413–429. CrossRef Medline

He L, Linden DJ, Sapirstein A (2012) Astrocyte inositol triphosphate receptor type 2 and cytosolic phospholipase A_2 alpha regulate asteriole responses in mouse neocortical brain slices. PLoS One 7:e42194. CrossRef Medline

Holtmaat A, Bonhoeffer T, Chow DK, Chuckowree J, De Paola V, Hofer SB, Hübener M, Keck T, Knott G, Lee WC, Mostany R, Mrsic-Flogel TD, Nedivi E, Portera-Cailliau C, Svoboda K, Trachtenberg JT, Wilbrecht L (2009) Long-term, high-resolution imaging in the mouse neocortex through a chronic cranial window. Nat Protoc 4:1128–1144. CrossRef Medline

Howarth C (2014) The contribution of astrocytes to the regulation of cerebral blood flow. Front Neurosci 8:103. CrossRef Medline

Kim SG, Ogawa S (2012) Biophysical and physiological origins of blood oxygenation level-dependent fMRI signals. J Cereb Blood Flow Metab 32:1188–1206. CrossRef Medline

Kocharyan A, Fernandes P, Tong XK, Vaucher E, Hamel E (2008) Specific subtypes of cortical GABA interneurons contribute to the neurovascular coupling response to basal forebrain stimulation. J Cereb Blood Flow Metab 28:221–231. CrossRef Medline

Kofuji P, Newman EA (2004) Potassium buffering in the central nervous system. Neuroscience 129:1045–1056. Medline

Langer J, Rose CR (2009) Synaptically induced sodium signals in hippocampal astrocytes in situ. J Physiol 587:5859–5877. CrossRef Medline

Li X, Zima AV, Sheikh F, Blatter LA, Chen J (2005) Endothelin-1-induced arrhythmogenic Ca2+ signaling is abolished in atrial myocytes of inositol-1,4,5-trisphosphate(IP3)-receptor type 2-deficient mice. Circ Res 96:1274–1281. CrossRef Medline

Lind BL, Brazhe AR, Jessen SB, Tan FC, Lauritzen MJ (2013) Rapid stimulus-evoked astrocyte Ca2+ elevations and hemodynamic responses in mouse somatosensory cortex in vivo. Proc Natl Acad Sci U S A 110:E4678–E4687. CrossRef Medline

Masamoto K, Fukuda M, Vazquez A, Kim SG (2009) Dose-dependent effect of isoflurane on neurovascular coupling in rat cerebral cortex. Eur J Neurosci 30:242–250. CrossRef Medline

Mathiisen TM, Lehre KP, Danbolt NC, Ottersen OP (2010) The perivascular astroglial sheath provides a complete covering of the brain microvessels: an electron microscopic 3D reconstruction. Glia 58:1094–1103. CrossRef Medline

McCaslin AF, Chen BR, Radosevich AJ, Cauli B, Hillman EM (2011) In vivo 3D morphology of astrocyte-vasculature interactions in the somatosensory cortex: implications for neurovascular coupling. J Cereb Blood Flow Metab 31:795–806. CrossRef Medline

Metea MR, Newman EA (2006) Glial cells dilate and constrict blood vessels: a mechanism of neurovascular coupling. J Neurosci 26:2862–2870. CrossRef Medline

Mishra A, Hamid A, Newman EA (2011) Oxygen modulation of neurovascular coupling in the retina. Proc Natl Acad Sci U S A 108:17827–17831. CrossRef Medline

Mulligan SJ, MacVicar BA (2004) Calcium transients in astrocyte endfeet cause cerebrovascular constrictions. Nature 431:195–199. CrossRef Medline

Navarrete M, Perea G, Fernandez de Sevilla D, Gómez-Gonzalo M, Núñez A, Martín ED, Araque A (2012) Astrocytes mediate in vivo cholinergic-induced synaptic plasticity. PLoS Biol 10:e1001259. CrossRef Medline

Newman EA (2005) Calcium increases in retinal glial cells evoked by light-induced neuronal activity. J Neurosci 25:5502–5510. CrossRef Medline

Newman EA (2013) Functional hyperemia and mechanisms of neurovascular coupling in the retinal vasculature. J Cereb Blood Flow Metab 33:1685–1695. CrossRef Medline

Nimmerjahn A, Kirchhoff F, Kerr JN, Helmchen F (2004) Sulforhodamine 101 as a specific marker of astroglia in the neocortex in vivo. Nat Methods 1:31–37. CrossRef Medline

Nizar K, Uhlirova H, Tian P, Saisan PA, Cheng Q, Reznichenko L, Weldy KL, Steed TC, Sridhar VB, MacDonald CL, Cui J, Gratiy SL, Sakadzić S, Boas DA, Beka TI, Einevoll GT, Chen J, Masliah E, Dale AM, Silva GA, et al. (2013) *In vivo* stimulus-induced vasodilation occurs without IP3 receptor activation and may precede astrocytic calcium increase. J Neurosci 33:8411–8422. CrossRef Medline

Nolte C, Matyash M, Pivneva T, Schipke CG, Ohlemeyer C, Hanisch UK, Kirchhoff F, Kettenmann H (2001) GFAP promoter-controlled EGFP-expressing transgenic mice: a tool to visualize astrocytes and astrogliosis in living brain tissue. Glia 33:72–86. CrossRef Medline

Panatier A, Vallée J, Haber M, Murai KK, Lacaille JC, Robitaille R (2011) Astrocytes are endogenous regulators of basal transmission at central synapses. Cell 146:785–798. CrossRef Medline

Paukert M, Agarwal A, Cha J, Doze VA, Kang JU, Bergles DE (2014) Norepinephrine controls astroglial responsiveness to local circuit activity. Neuron 82:1263–1270. CrossRef Medline

Paulson OB, Newman EA (1987) Does the release of potassium from astrocyte endfeet regulate cerebral blood flow? Science 237:896–898. CrossRef Medline

Petravicz J, Fiacco TA, McCarthy KD (2008) Loss of IP3 receptor-dependent Ca^{2+} increases in hippocampal astrocytes does not affect baseline CA1 pyramidal neuron synaptic activity. J Neurosci 28:4967–4973. CrossRef Medline

Petzold GC, Murthy VN (2011) Role of astrocytes in neurovascular coupling. Neuron 71:782–797. CrossRef Medline

Porter JT, McCarthy KD (1996) Hippocampal astrocytes *in situ* respond to

glutamate released from synaptic terminals. J Neurosci 16:5073–5081. Medline

Roy CS, Sherrington CS (1890) On the regulation of the blood-supply of the brain. J Physiol 11:85–158.17. Medline

Schaffer CB, Friedman B, Nishimura N, Schroeder LF, Tsai PS, Ebner FF, Lyden PD, Kleinfeld D (2006) Two-photon imaging of cortical surface microvessels reveals a robust redistribution in blood flow after vascular occlusion. PLoS Biol 4:e22. CrossRef Medline

Schulz K, Sydekum E, Krueppel R, Engelbrecht CJ, Schlegel F, Schröter A, Rudin M, Helmchen F (2012) Simultaneous BOLD fMRI and fiber-optic calcium recording in rat neocortex. Nat Methods 9:597–602. CrossRef Medline

Schummers J, Yu H, Sur M (2008) Tuned responses of astrocytes and their influence on hemodynamic signals in the visual cortex. Science 320:1638–1643. CrossRef Medline

Shigetomi E, Tong X, Kwan KY, Corey DP, Khakh BS (2012) TRPA1 channels regulate astrocyte resting calcium and inhibitory synapse efficacy through GAT-3. Nat Neurosci 15:70–80. CrossRef Medline

Shigetomi E, Bushong EA, Haustein MD, Tong X, Jackson-Weaver O, Kracun S, Xu J, Sofroniew MV, Ellisman MH, Khakh BS (2013) Imaging calcium microdomains within entire astrocyte territories and endfeet with GCaMPs expressed using adeno-associated viruses. J Gen Physiol 141:633–647. CrossRef Medline

Stobart JL, Lu L, Anderson HD, Mori H, Anderson CM (2013) Astrocyte-induced cortical vasodilation is mediated by D-serine and endothelial nitric oxide synthase. Proc Natl Acad Sci U S A 110:3149–3154. CrossRef Medline

Straub SV, Bonev AD, Wilkerson MK, Nelson MT (2006) Dynamic inositol trisphosphate-mediated calcium signals within astrocytic endfeet underlie vasodilation of cerebral arterioles. J Gen Physiol 128:659–669. CrossRef Medline

Sun MY, Devaraju P, Xie AX, Holman I, Samones E, Murphy TR, Fiacco TA (2014) Astrocyte calcium microdomains are inhibited by Bafilomycin A1 and cannot be replicated by low-level Schaffer collateral stimulation in situ. Cell Calcium 55:1–16. CrossRef Medline

Sun W, McConnell E, Pare JF, Xu Q, Chen M, Peng W, Lovatt D, Han X, Smith Y, Nedergaard M (2013) Glutamate-dependent neuroglial calcium signaling differs between young and adult brain. Science 339:197–200. CrossRef Medline

Takano T, Tian GF, Peng W, Lou N, Libionka W, Han X, Nedergaard M (2006) Astrocyte-mediated control of cerebral blood flow. Nat Neurosci 9:260–267. CrossRef Medline

Takano T, He W, Han X, Wang F, Xu Q, Wang X, Oberheim Bush NA, Cruz N, Dienel GA, Nedergaard M (2014) Rapid manifestation of reactive astrogliosis in acute hippocampal brain slices. Glia 62:78–95. CrossRef Medline

Takata N, Mishima T, Hisatsune C, Nagai T, Ebisui E, Mikoshiba K, Hirase H (2011) Astrocyte calcium signaling transforms cholinergic modulation to cortical plasticity *in vivo*. J Neurosci 31:18155–18165. CrossRef Medline

Takata N, Nagai T, Ozawa K, Oe Y, Mikoshiba K, Hirase H (2013) Cerebral blood flow modulation by basal forebrain or whisker stimulation can occur independently of large cytosolic Ca^{2+} signaling in astrocytes. PLoS One 8:e66525. CrossRef Medline

Thrane AS, Rangroo Thrane V, Zeppenfeld D, Lou N, Xu Q, Nagelhus EA, Nedergaard M (2012) General anesthesia selectively disrupts astrocyte calcium signaling in the awake mouse cortex. Proc Natl Acad Sci U S A 109:18974–18979. CrossRef Medline

Tian P, Teng IC, May LD, Kurz R, Lu K, Scadeng M, Hillman EM, De Crespigny AJ, D'Arceuil HE, Mandeville JB, Marota JJ, Rosen BR, Liu TT, Boas DA, Buxton RB, Dale AM, Devor A (2010) Cortical depth-specific microvascular dilation underlies laminar differences in blood oxygenation level-dependent functional MRI signal. Proc Natl Acad Sci U S A 107:15246–15251. CrossRef Medline

Volterra A, Liaudet N, Savtchouk I (2014) Astrocyte Ca(2)(+) signalling: an unexpected complexity. Nat Rev Neurosci 15:327–335. CrossRef Medline

Wang F, Smith NA, Xu Q, Fujita T, Baba A, Matsuda T, Takano T, Bekar L, Nedergaard M (2012) Astrocytes modulate neural network activity by Ca(2)+-dependent uptake of extracellular K+. Sci Signal 5:ra26. CrossRef Medline

Wang F, Smith NA, Xu Q, Goldman S, Peng W, Huang JH, Takano T, Nedergaard M (2013) Photolysis of caged Ca^{2+} but not receptor-mediated Ca^{2+} signaling triggers astrocytic glutamate release. J Neurosci 33:17404–17412. CrossRef Medline

Wang X, Lou N, Xu Q, Tian GF, Peng WG, Han X, Kang J, Takano T, Nedergaard M (2006) Astrocytic Ca2+ signaling evoked by sensory stimulation in vivo. Nat Neurosci 9:816–823. CrossRef Medline

Wess J, Nakajima K, Jain S (2013) Novel designer receptors to probe GPCR signaling and physiology. Trends Pharmacol Sci 34:385–392. CrossRef Medline

Winship IR, Plaa N, Murphy TH (2007) Rapid astrocyte calcium signals correlate with neuronal activity and onset of the hemodynamic response *in vivo*. J Neurosci 27:6268–6272. CrossRef Medline

Witthoft A, Filosa JA, Karniadakis GE (2013) Potassium buffering in the neurovascular unit: models and sensitivity analysis. Biophys J 105:2046–2054. CrossRef Medline

Xu HT, Pan F, Yang G, Gan WB (2007) Choice of cranial window type for in vivo imaging affects dendritic spine turnover in the cortex. Nat Neurosci 10:549–551. CrossRef Medline

Yang G, Pan F, Parkhurst CN, Grutzendler J, Gan WB (2010) Thinned-skull cranial window technique for long-term imaging of the cortex in live mice. Nat Protoc 5:201–208. CrossRef Medline

Zhou M, Xu G, Xie M, Zhang X, Schools GP, Ma L, Kimelberg HK, Chen H (2009) TWIK-1 and TREK-1 are potassium channels contributing significantly to astrocyte passive conductance in rat hippocampal slices. J Neurosci 29:8551–8564. CrossRef Medline

Zonta M, Angulo MC, Gobbo S, Rosengarten B, Hossmann KA, Pozzan T, Carmignoto G (2003) Neuron-to-astrocyte signaling is central to the dynamic control of brain microcirculation. Nat Neurosci 6:43–50. Medline